

Performance Analysis of RIS-Assisted Spectrum Sharing Systems

Yazan H. Al-Badarneh, *Member, IEEE*, Mustafa K. Alshawaqfeh, *Member, IEEE*, Osamah S. Badarneh, *Member, IEEE*, Yazid M. Khattabi, *Member, IEEE*

Abstract—We propose a reconfigurable intelligent surface (RIS)-assisted underlay spectrum sharing system, in which a RIS-assisted secondary network shares the spectrum licensed for a primary network. The secondary network consists of a secondary source (SS), an RIS, and a secondary destination (SD), operating in a Rician fading environment. We study the performance of the secondary network while considering a peak power constraint at the SS and an interference power constraint at the primary receiver (PR). Initially, we characterize the statistics of the signal-to-noise ratio (SNR) of the RIS-assisted secondary network by deriving novel analytical expressions for the cumulative distribution function (CDF) and probability density function (PDF) in terms of the incomplete H -function. Building upon the SNR statistics, we analyze the outage probability, ergodic capacity, and average bit error rate, subsequently deriving novel exact expressions for these performance measures. Furthermore, we obtain novel asymptotic expressions for the performance measures of interest when the peak power of the SS is high. Finally, we conduct exhaustive Monte-Carlo simulations to confirm the correctness of our theoretical analysis.

Index Terms—Reconfigurable intelligent surfaces; spectrum sharing; 6G wireless communications; performance analysis

I. INTRODUCTION

Since the advent of its first commercial version in 2018, and as compared to its previous generations, the fifth generation (5G) has shaped a distinguished paradigm of mobile communications with the following emerged applications; namely, enhanced mobile broadband (eMBB), ultrareliable low-latency communications (URLLC) and massive machine-type communications (mMTC) [1], [2]. However, the ever-increasing current data-hungry applications, such as online gaming, high-definition video streaming, holographic videos, smart homes, mobile shopping, etc., has tremendously augmented the wireless data traffic volume to the extent that 5G would not be capable to support in the coming few years. Motivated by this challenge, industry and academia have recently started conceptualizing the next generation (the sixth generation (6G)) of wireless communication systems aimed at supporting communication services for future wireless requirements and applications [3].

Y. H. Al-Badarneh and Y. M. Khattabi are with the Department of Electrical Engineering, The University of Jordan, Amman, 11942 (email: yalbadarneh, y.khattabi@ju.edu.jo).

Y. M. Khattabi is with College of Engineering and Technology, American University of the Middle East, Egaila 54200, Kuwait. e-mail: yazid.khattabi@aum.edu.kw.

O. S. Badarneh and M. K. Alshawaqfeh are with the Electrical Engineering Department, School of Electrical Engineering and Information Technology, German Jordanian University, Amman 11180, Jordan (e-mail: Osamah.Badarneh, mustafa.shawaqfeh@gnu.edu.jo).

The 6G is expected to provide huge data coverage and to allow tremendous number of subscribers and congested areas of small devices to be connected efficiently and with unconventional high data rate speeds. Nevertheless, attaining all of these 6G expected requirements and supporting all its applications, no wonder, requires multiple enabling technologies along with radical solutions to all arising communication engineering challenges, especially, those related to physical layer aspects and fading environments. The random nature of fading environments and the disruptive interactions of the propagated waves with the adjacent objects are the main causes of signals degradation in wireless communication systems. In this context, and within the scope of smart radio environments, there is an increasing interest in proposing creative communication schemes in which the randomness of the fading environment is to be utilized to improve received signals quality. A brand-new example is the technology of reconfigurable intelligent surfaces (RISs), which have been designed to allow network operators to control reflection, refraction, and scattering characteristics of propagated radio waves in a manner yielding to reducing the negative impacts of fading environments and improving received signals quality [4]- [6].

The RISs are surfaces implemented from electromagnetic (EM) materials that can be electronically tuned to control the amplitude, phase, frequency, and polarization (wavefront) of propagated signals without the need to complex decoding and encoding processes [7]- [9]. In addition, RISs are nearly passive entities, do not require dedicated power sources, can be deployed easily, do not produce noise, and provide full-duplex transmission; traits that are readily essential to support various applications in 6G networks. All of these distinguishable aspects have made RISs one of the most recent attractive technologies in both academia and industry. In the following, we review the literature of RIS-assisted wireless communications from a performance analysis perspective.

A. Performance of RIS-assisted systems

In [10], the error performance of RIS-assisted communication systems is studied, where the maximized end-to-end (e2e) signal-to-noise ratio (SNR) of RIS-assisted networks is assumed to follow a non-central chi-square random variable (RV) thanks to the central limit theorem (CLT). Based on the SNR statistics, the average symbol error probability (SEP) for M-ary phase shift keying (PSK) and square M-ary quadrature amplitude modulation (M-QAM) are investigated.

Accurate analytical approximations to the distributions of the received SNR for different RIS-based wireless system setups are provided in [11]. In addition, closed-form and asymptotic expressions for the average channel capacity and the average bit error rate (BER) are derived. The outage probability and the achievable diversity of RIS-assisted communication systems over generalized fading channels and under the effect of phase noise are investigated in [12]. The ergodic capacity and the average symbol error rate (SER) of RIS-aided systems over Rayleigh fading channels have been studied in [13]. Very recently, a stochastic geometry approach was adopted to assess the coverage probability and average achievable rate of RIS-assisted large-scale networks [14].

RIS-assisted networks over Rician fading channels have gained much attention recently [15]- [20]. The Rician model is more general than Rayleigh model and is desirable in realistic communication settings to account for the existence of Line-of-Sight (LOS) components between the transmitter and the RIS, and between the RIS and the receiver. In [15], the authors analyze the ergodic capacity and the outage probability of RIS-aided single-input single-output (SISO) systems over Rician fading channels and in the presence of a direct channel between the transmitter and receiver. In [16], authors study the error performance, data rate of RIS-aided systems with single or multiple RISs in indoor and outdoor environments. Highly accurate closed-form approximations for the e_2e SNR statistics of RIS-assisted networks in Rician fading are derived in [17]. The authors build upon the obtained statistics to derive closed-form expressions for the ergodic capacity and the average SER. The outage performance of RIS-aided systems with statistical channel state information (CSI) under the Rician fading model is investigated [18]. A closed-form expression for the outage probability in terms of Marcum Q-function is derived. Very recently, the authors in [19] derive exact analytical expressions for the outage probability, the ergodic capacity, and the average BER of RIS-aided communications over the sum of cascaded Rician channels. In [20], a robust and secure multiuser multiple-input single-output (MISO) downlink systems self-sustainable RIS was considered. The authors explored the joint optimization of beamformers at an access point (AP) and the phase shifts, along with the energy harvesting schedule at the RIS, aiming to maximize the overall system sum rate.

B. Spectrum sharing systems

The tremendously increasing number of communicating devices in future 6G wireless communications will undoubtedly lead to spectrum scarcity, which is a significant problem in modern wireless networks [21]. Spectrum scarcity can be addressed through spectrum sharing-empowered techniques, in which, same frequency band can be shared by multiple communicating devices, but under some interference management mechanisms. In this context, cognitive radio (CR) is defined as an efficient spectrum sharing technique that allows secondary network devices to wisely share same frequency bands licensed for primary network devices [22], [23]. In CR systems, two main spectrum sharing modes can be employed: (i) the overlay mode and (ii) the underlay mode [24]. In

the overlay mode, secondary devices utilize frequency bands unoccupied by idle primary devices to accomplish their data transmissions. Nevertheless, in the underlay mode, secondary devices perform their data transmissions simultaneously with primary devices, but with limited transmit power such that the interference at primary devices does not exceed a predefined level.

Envisioning RIS technology in underlay CR networks has attracted much research interest recently as an efficient solution to improve the performance of such networks. For instance, the RIS has been considered as an indispensable approach to further enhance the energy and spectrum efficiency in CR networks [25], [26]. In addition, the deployment of the RIS in CR networks can significantly enhance the secrecy outage probability and the achievable secrecy rate [27], [28]. In what follows, we provide a comprehensive literature review on RIS-aided CR systems.

The RIS technology is employed to aid multiple-input multiple-output (MIMO) downlink (DL) communication in CR systems [25], where the achievable weighted sum rate of the secondary users is maximized under a transmit power limit at the secondary transmitter (ST), interference temperature constraints on the primary users (PUs), and unit modulus constraints. In [26], the authors propose multiple RISs to assist the DL communication of MISO CR systems. The achievable rate of secondary user (SU) is maximized subject to a transmit power limit at the ST and interference temperature constraints on the PUs. In [29], the authors consider a resource allocation problem for multiuser full-duplex (FD) CR systems in the presence of a RIS. The study aimed to maximize the sum rate by collectively optimizing the DL transmit beamforming and uplink (UL) receive beamforming vectors, the transmit power of the UL users, and the phase shift matrix at the RIS. In [30], the authors suggest and examine two separate configurations of RIS deployment to improve the performance of CR networks. Analytical expressions for the false alarm and detection probabilities of the two RIS configurations are obtained. In [31], a robust beamforming design is proposed for RIS-aided CR systems. The authors investigated the beamforming design considering two types of error models for PU-related channels: (i) bounded CSI and (ii) statistical CSI.

C. Contributions

In the context of performance analysis, most of the aforementioned works consider the performance of RIS-assisted traditional communication systems with no spectrum sharing, where the Rayleigh and Rician fading models are considered. In the context of RIS-aided spectrum sharing systems, all previous works focus on resource allocation problems to optimize the performance of the secondary network in terms of data rate. The deployment of the RIS in spectrum sharing systems can substantially improve the performance with regard to the outage probability, ergodic capacity, and average BER.

Only a few studies have recently focused on analyzing the performance in terms of the outage probability of RIS-aided spectrum sharing systems. For instance, the outage probability analysis of a simultaneously transmitting and reflecting reconfigurable intelligent surface (STAR-RIS)-empowered cognitive

non-terrestrial vehicle network with non-orthogonal multiple access (NOMA) was considered in [32]. The outage probability of a RIS-aided cognitive radio network where the RIS is used only to eliminate the interference from the secondary transmitter to the primary receiver was studied in [33]. Very recently, the characteristics of the signal-to-Interference-plus-Noise Ratio (SINR) of a RIS-aided device-to-device (D2D) communication system operating in underlay mode was considered in [34]. The authors therein considered a novel SINR maximization problem that jointly optimizes transmit power budget at the D2D source and the RIS deployment.

In this work, we present a novel RIS-assisted underlay spectrum sharing system, in which a secondary network assisted by a RIS shares the spectrum dedicated to a primary network. The secondary network comprises a secondary source (SS), a RIS, and a secondary destination (SD), operating in a Rician fading environment. This work aims to provide a comprehensive performance of the envisioned RIS-assisted secondary network. To the best of the authors' knowledge, such a comprehensive performance analysis has not been addressed in the existing literature. The advantages of the proposed system lie in the following aspects:

- The RIS-assisted secondary network shares the spectrum of the primary network without deteriorating the performance of the primary link. This can be ensured by adopting transmit power adaptation at the SS. In particular, the SS can adjust its transmit power appropriately to limit the interference power at the primary receiver (PR) caused by the SS to below a specified threshold. Additionally, the transmit power of the SS is subject to a peak power constraint P .
- The deployment of the RIS in the secondary network is of significant practical importance due to the following reasons:
 - In a situation where no direct link is available between the SS and the SD, the RIS is deployed in an effort to make the communication between the SS and the SD not only possible but also reliable.
 - Unlike relaying [13] and backscatter [35] communication techniques, the reflected wave from the RIS can be effectively controlled and programmed in real-time due to the adjustable phase shifts of the RIS. The RIS is mainly deployed for receiving a signal from the SS and focusing the reflected signal towards the SD exclusively. As a result, any interference signal reflected from the RIS towards the PR is disregarded due to the limited coverage area of the RIS, which restricts the propagation of interference towards the PR [33], [34] and [36].
- The RIS-assisted secondary network is assumed to undergo Rician fading. The Rician model is more general than Rayleigh model and is desirable in realistic communication settings to account for the existence of LOS components between the SS and RIS, and between the RIS and the SD [17]. The widely adopted Rayleigh fading model is a special case of the Rician model when the Rician K -factor equals zero.

It is worth emphasizing that expressing the cumulative distribution function (CDF) and probability density function (PDF) of the SNR in the RIS-assisted secondary network, while considering both the Rician model and the transmit power adaption at the SS, in closed-form is very challenging. Consequently, the performance analysis is mathematically intricate, requiring the solution of difficult integrals to quantify the ergodic capacity and the average BER. Such integrals are tackled using the theory of the incomplete H -function. To our best knowledge, this work represents the first application of the incomplete H -function in analyzing wireless communication systems. The key contributions of this work can be outlined as follows:

- In terms of an incomplete H -function, we develop novel analytical expressions for the CDF and PDF of the SNR. The outage probability can be evaluated immediately afterward using the provided CDF.
- Building upon the obtained PDF and CDF, we provide the cumbersome ergodic capacity and average BER analysis. Novel analytical expressions in terms of the incomplete H -function and the H -function are obtained.
- Utilizing the asymptotic properties of the incomplete H -function, we obtain accurate asymptotic expressions for the outage probability, ergodic capacity, and the average BER when the peak power of the SS is high.

The subsequent content of this work is organized as follows. The system model is articulated in Section II. The exact and the asymptotic performance of the RIS-assisted secondary network are investigated in Section III and Section IV, respectively. Section V is dedicated to investigating the numerical results. Finally, the conclusions are drawn in Section VI.

II. SYSTEM MODEL

We take into consideration an underlay spectrum sharing system, as shown in Fig. 1, where a secondary network shares the spectrum allotted to a primary network comprising M PTs simultaneously communicating with a PR. The PTs and the PR are single-antenna devices. The secondary network is a RIS-assisted environment consisting of a SS, an RIS of N reflecting elements, and a SD. The SS and the SD are single-antenna terminals. We use h_0 to denote the channel coefficient from the SS to the PR. For the secondary network, we denote the channel coefficients from the SS to the n^{th} reflecting element and from the n^{th} reflecting element to the SD by h_n and g_n , respectively. The channel coefficients of the secondary network can be expressed as $h_n = \alpha_n e^{-j\theta_n}$ and $g_n = \beta_n e^{-j\psi_n}$, where α_n and β_n represent the channel envelopes, and θ_n and ψ_n represent the phase shifts. The envelopes α_n and β_n are independent random variables (RVs), for $n = 1, 2, \dots, N$.

We assume that the SS will communicate with the SD through the RIS, without a direct link between the SS and the SD due to presence of natural or man-made obstacles [10], [17] and [37]. Additionally, we take into account the existence of a LOS component between the SS and the RIS, and between the RIS and the SD. Accordingly, α_n , $n = 1, 2, \dots, N$ can be modeled as independent identically

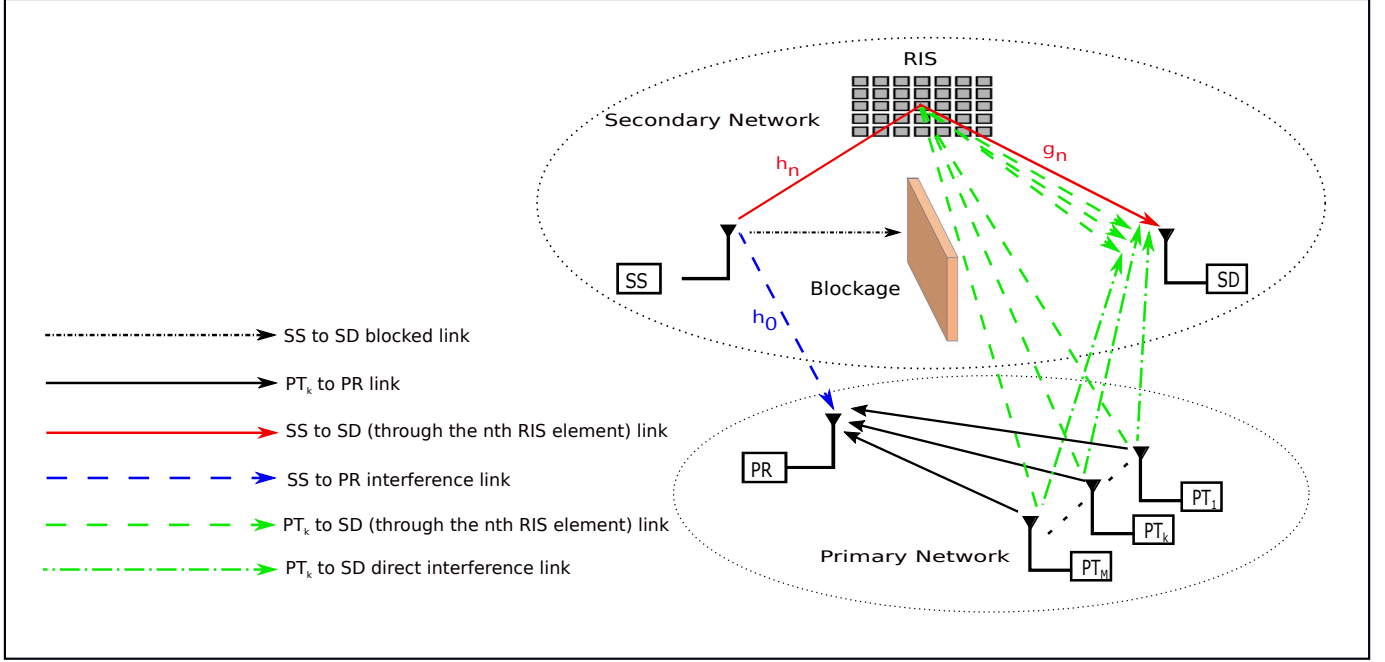


Fig. 1. A RIS-aided secondary network shares the spectrum allocated to a primary network consisting of M PTs simultaneously communicating with a PR.

distributed (i.i.d) Rician RVs with shape parameter K_1 and scale parameter Ω_1 . Similarly, β_n , $n = 1, 2, \dots, N$ can be also viewed as i.i.d Rician RVs with shape parameter K_2 and scale parameter Ω_2 ¹. The shape parameter and scale parameter can be, respectively, characterized as $K_j = \frac{\mu_j^2}{2\sigma_j^2}$ and $\Omega_j = \mu_j^2 + 2\sigma_j^2$, $j \in \{1, 2\}$, where μ_j^2 denotes the power in LOS component and $2\sigma_j^2$ denotes the power in the Non-Line of Sight (NLOS) component.

To this end, we assume that the primary and secondary networks are distant from each other. Accordingly, $|h_0|$ can be presumed to undergo Rayleigh fading implying that $|h_0|^2$ is an exponential RV with mean λ . Furthermore, we assume that the interference caused by the PTs to the SD (i.e., direct PTs \rightarrow SD and PTs \rightarrow RIS \rightarrow SD) is translated into white Gaussian noise at the SD. This assumption is justified by the central limit theorem (CLT), which indicates that the interference from multiple PTs converges to a Gaussian distribution due to the presence of multiple PTs and multiple RIS elements [38]. Accordingly, the interference-plus-noise at the SD can be effectively modeled as an additive white Gaussian noise (AWGN) with a zero mean and variance of N_0 .

As shown in [10], the instantaneous SNR at the SD is maximized by eliminating the channel phase shifts ψ_n and θ_n . Hence, the maximized instantaneous SNR at the SD, denoted

by ρ , is given by²

$$\rho = \frac{P_s \left(\sum_{n=1}^N \alpha_n \beta_n \right)^2}{N_0}, \quad (1)$$

where P_s is the transmit power of the SS.

In spectrum sharing systems, the PR mandates that the instantaneous interference caused by the SS is below predetermined threshold Q , which indicates the interference power limit at the PR³. Meanwhile, the transmit power of the SS is subject to a peak power constraint P . Accordingly, the transmit power at the SS is given by

$$P_s = \min \left(\frac{Q}{|h_0|^2}, P \right), \quad (2)$$

where P is the peak power of the SS. Capitalizing on (2), ρ in (1) can be rewritten as

$$\rho = \min \left(\frac{Q}{|h_0|^2}, P \right) \frac{R^2}{N_0} = \begin{cases} PR^2, & |h_0|^2 \leq \frac{Q}{P} \\ \frac{QR^2}{|h_0|^2}, & |h_0|^2 > \frac{Q}{P} \end{cases}, \quad (3)$$

where $R^2 = \left(\sum_{n=1}^N \alpha_n \beta_n \right)^2$, and N_0 is set to unity without loss of generality.

¹The assumption of i.i.d RIS channels has been widely adopted in the literature since it facilitates the development of mathematically tractable formulations and serves as a foundational framework for understanding the performance. The consideration of correlated RIS Rician channels requires the development of different mathematical formulations, which remains as a future research endeavor.

²Similar to [10], [11] and [17], perfect knowledge of the RIS channels CSI is assumed to be available at the SS. Furthermore, perfect CSI can be acquired at the transmitter- or the receiver-side [39], [40]. The impact of imperfect CSI is beyond the scope of this work and is left as a future research endeavor.

³The interference signal reflected from the RIS towards the PR is disregarded due to the limited coverage area of the RIS, which restricts the propagation of interference towards the PR [33], [34] and [36].

To this end, the CDF of R^2 is given by [17, Theorem 1]

$$F_{R^2}(z) = \frac{\gamma\left(v, \frac{\sqrt{z}}{b}\right)}{\Gamma(v)}, \quad z \geq 0, \quad (4)$$

where $\gamma(\cdot, \cdot)$ is the lower incomplete gamma function [41, Eq. (8.350.1)]. If we define $R_n = \alpha_n \beta_n$, where R_n are i.i.d RVs, $n = 1, 2, \dots, N$, then the parameters v and b are dependent on the mean and variance of R_n , and can be respectively expressed as [17]

$$v = \frac{N(E[R_n])^2}{\text{var}(R_n)}, \quad b = \frac{\text{var}(R_n)}{E[R_n]},$$

where $E[R_n]$ and $\text{var}(R_n)$ are obtained as in [17, Eq. (4)] and [17, Eq. (5)], respectively.

III. EXACT PERFORMANCE ANALYSIS

This section provides the performance of the RIS-assisted secondary network. We start with deriving analytical expressions for the CDF and PDF of the maximized instantaneous SNR ρ in (3). The derived expressions are to be utilized in the sequel to analyze the outage performance, ergodic capacity and average BER performance.

A. SNR Statistics

In Theorem 1 below, the CDF and PDF of ρ are provided in terms of incomplete H -functions.

Theorem 1: The CDF and PDF of ρ are, respectively, given by

$$F_\rho(z) = \frac{\gamma\left(v, \sqrt{\frac{z}{b^2 P}}\right)}{\Gamma(v)} \left(1 - e^{-\frac{Q}{P\lambda}}\right) + \frac{1}{\Gamma(v)} \Gamma_{2,2}^{1,2} \left[\sqrt{\frac{z\lambda}{b^2 Q}} \mid \begin{matrix} (0, \frac{1}{2}, \frac{Q}{P\lambda}), (1, 1) \\ (v, 1), (0, 1) \end{matrix} \right], \quad (5)$$

and

$$f_\rho(z) = \frac{z^{\frac{v}{2}-1} e^{-\sqrt{\frac{z}{b^2 P}}}}{2(b^2 P)^{\frac{v}{2}} \Gamma(v)} \left(1 - e^{-\frac{Q}{P\lambda}}\right) + \frac{z^{-1}}{\Gamma(v)} \Gamma_{3,3}^{1,3} \left[\sqrt{\frac{z\lambda}{b^2 Q}} \mid \begin{matrix} (0, \frac{1}{2}, \frac{Q}{P\lambda}), (0, \frac{1}{2}), (1, 1) \\ (v, 1), (0, 1), (1, \frac{1}{2}) \end{matrix} \right], \quad (6)$$

where $\Gamma_{p,q}^{m,n}(\cdot)$ is the incomplete H -function [42, Eq. (2.3)] and $\Gamma(\cdot)$ is the gamma function [43, Eq. (8.310.1)].

Proof: See Appendix A.

B. Outage Probability

A fundamental measure of the communication link reliability is the outage probability, which is defined as the probability that the received SNR falls below a predefined threshold γ_{th} . Correspondingly, the outage probability of the secondary network, denoted by $P_{\text{out}}(\gamma_{\text{th}})$, is given by

$$P_{\text{out}}(\gamma_{\text{th}}) = F_\rho(\gamma_{\text{th}}) = \frac{\gamma\left(v, \sqrt{\frac{\gamma_{\text{th}}}{b^2 P}}\right)}{\Gamma(v)} \left(1 - e^{-\frac{Q}{P\lambda}}\right) + \frac{1}{\Gamma(v)} \Gamma_{2,2}^{1,2} \left[\sqrt{\frac{\gamma_{\text{th}}\lambda}{b^2 Q}} \mid \begin{matrix} (0, \frac{1}{2}, \frac{Q}{P\lambda}), (1, 1) \\ (v, 1), (0, 1) \end{matrix} \right]. \quad (7)$$

C. Ergodic Capacity

We now provide the ergodic capacity analysis of the secondary network under consideration. The instantaneous capacity of the secondary network for a given realization of the RV ρ , denoted by C_ρ , is given by [44]

$$C_\rho = \log_2(1 + \rho) \quad [\text{bits/s/Hz}]. \quad (8)$$

In what follows, we use C to denote the ergodic capacity, which can be obtained by averaging over all realizations of the RV ρ as

$$C = E[\log_2(1 + \rho)] = \frac{1}{\ln(2)} \int_0^\infty \ln(1 + z) f_\rho(z) dz, \quad (9)$$

where $f_\rho(z)$ is as given in (6).

In Theorem 2 below, the ergodic capacity is derived in terms of the H -function and the incomplete H -function.

Theorem 2: The ergodic capacity of the secondary network is given by

$$C = C^{(1)} + C^{(2)}, \quad (10)$$

where $C^{(1)}$ and $C^{(2)}$ are, respectively, given by

$$C^{(1)} = \frac{(1 - e^{-\frac{Q}{P\lambda}})}{\Gamma(v) \ln(2)} H_{3,2}^{1,3} \left[b^2 P \mid \begin{matrix} (1-v, 2), (1, 1), (1, 1) \\ (1, 1), (0, 1) \end{matrix} \right], \quad (11)$$

$$C^{(2)} = \frac{1}{\ln(2) \Gamma(v)} \Gamma_{3,3}^{2,3} \left[\sqrt{\frac{\lambda}{b^2 Q}} \mid \begin{matrix} (0, \frac{1}{2}, \frac{Q}{P\lambda}), (1, \frac{1}{2}), (1, 1) \\ (v, 1), (1, \frac{1}{2}), (0, 1) \end{matrix} \right], \quad (12)$$

where $H_{p,q}^{m,n}[\cdot]$ is the univariate H -function [45, Eq. (1.2)].

Proof: See Appendix B.

D. Average BER

Here, we study the average BER of the secondary network. We focus on various binary modulation formats with conditional BER, denoted by $P_e(\rho)$, is given by [46]

$$P_e(\rho) = \frac{\Gamma(\zeta, \delta\rho)}{2\Gamma(\zeta)}, \quad (13)$$

where ρ is the instantaneous SNR in (3), and $\Gamma(\cdot, \cdot)$ is the upper incomplete gamma function [41, Eq. (8.350.2)], and the parameters δ and ζ are modulation-specific constants. The average BER, denoted by P_e , can be derived as [46]

$$P_e = \frac{\delta^\zeta}{2\Gamma(\zeta)} \int_0^\infty e^{-\delta z} z^{\zeta-1} F_\rho(z) dz. \quad (14)$$

In Theorem 3 below, we obtain the average BER of the secondary network in terms of the H -function and the incomplete H -function.

Theorem 3: The average BER of the secondary network is given by

$$P_e = P_e^{(1)} + P_e^{(2)}, \quad (15)$$

where $P_e^{(1)}$ and $P_e^{(2)}$ are, respectively, given by

$$P_e^{(1)} = \frac{(1 - e^{-\frac{Q}{P\lambda}})}{2\Gamma(v)\Gamma(\zeta)} H_{2,2}^{1,2} \left[\sqrt{\frac{1}{\delta b^2 P}} \mid \begin{matrix} (1-\zeta, \frac{1}{2}), (1, 1) \\ (v, 1), (0, 1) \end{matrix} \right], \quad (16)$$

$$P_e^{(2)} = \frac{1}{2\Gamma(v)\Gamma(\zeta)} \Gamma_{3,2}^{1,3} \left[\sqrt{\frac{\lambda}{\delta b^2 Q}} \middle| \begin{matrix} (0, \frac{1}{2}, \frac{Q}{P\lambda}), (1-\zeta, \frac{1}{2}), (1,1) \\ (v,1), (0,1) \end{matrix} \right]. \quad (17)$$

Proof: See Appendix C.

IV. ASYMPTOTIC PERFORMANCE ANALYSIS

This section provides the asymptotic performance of the secondary network at high values of peak power P . While the exact results obtained in the previous section are general enough to cover various arbitrary values of system parameters, the results of this section are of interest when $P\lambda \gg Q$. In what follows, we derive asymptotic expressions for the outage probability, ergodic capacity, and average BER when $P\lambda \gg Q$.

A. Asymptotic Outage Probability

Considering $P_{out}(\gamma_{th})$ in (7), the first term will approach zero when $P\lambda \gg Q$ (i.e., $(1 - e^{-\frac{Q}{P\lambda}}) \rightarrow 0$). Hence, the asymptotic outage probability, denoted by $P_{out}^{asy}(\gamma_{th})$, can be approximated as

$$P_{out}^{asy}(\gamma_{th}) \approx \frac{1}{\Gamma(v)} \Gamma_{2,2}^{1,2} \left[\sqrt{\frac{\gamma_{th}\lambda}{b^2 Q}} \middle| \begin{matrix} (0, \frac{1}{2}, \frac{Q}{P\lambda}), (1,1) \\ (v,1), (0,1) \end{matrix} \right]. \quad (18)$$

If we further consider the unlimited peak power scenario (i.e., $P \rightarrow \infty$), then $P_{out}^{asy}(\gamma_{th})$ can be obtained as

$$P_{out}^{asy}(\gamma_{th}) \approx \frac{1}{\Gamma(v)} \Gamma_{2,2}^{1,2} \left[\sqrt{\frac{\gamma_{th}\lambda}{b^2 Q}} \middle| \begin{matrix} (0, \frac{1}{2}, 0), (1,1) \\ (v,1), (0,1) \end{matrix} \right]. \quad (19)$$

In view of [47, case (4)], the incomplete H -function in (19) reduces to an H -function as

$$P_{out}^{asy}(\gamma_{th}) \approx \frac{1}{\Gamma(v)} H_{2,2}^{1,2} \left[\sqrt{\frac{\gamma_{th}\lambda}{b^2 Q}} \middle| \begin{matrix} (0, \frac{1}{2}), (1,1) \\ (v,1), (0,1) \end{matrix} \right]. \quad (20)$$

B. Asymptotic Capacity

When $P\lambda \gg Q$, the asymptotic ergodic capacity, denoted by C^{asy} , can be approximated by $C^{(2)}$ in (12). The term $C^{(1)}$ in (11) becomes negligible due to $(1 - e^{-\frac{Q}{P\lambda}}) \rightarrow 0$. Accordingly,

$$C^{asy} \approx \frac{1}{\ln(2)\Gamma(v)} \Gamma_{3,3}^{2,3} \left[\sqrt{\frac{\lambda}{b^2 Q}} \middle| \begin{matrix} (0, \frac{1}{2}, \frac{Q}{P\lambda}), (1, \frac{1}{2}), (1,1) \\ (v,1), (1, \frac{1}{2}), (0,1) \end{matrix} \right]. \quad (21)$$

If we further consider the unlimited peak power scenario (i.e., $P \rightarrow \infty$), then

$$\begin{aligned} C^{asy} &\approx \frac{1}{\ln(2)\Gamma(v)} \Gamma_{3,3}^{2,3} \left[\sqrt{\frac{\lambda}{b^2 Q}} \middle| \begin{matrix} (0, \frac{1}{2}, 0), (1, \frac{1}{2}), (1,1) \\ (v,1), (1, \frac{1}{2}), (0,1) \end{matrix} \right] \\ &= \frac{1}{\ln(2)\Gamma(v)} H_{3,3}^{2,3} \left[\sqrt{\frac{\lambda}{b^2 Q}} \middle| \begin{matrix} (0, \frac{1}{2}), (1, \frac{1}{2}), (1,1) \\ (v,1), (1, \frac{1}{2}), (0,1) \end{matrix} \right]. \end{aligned} \quad (22)$$

C. Asymptotic Average BER

Following the same procedure for deriving the P_{out}^{asy} , and C^{asy} , the asymptotic BER, denoted by P_e^{asy} , can be obtained as

$$P_e^{asy} \approx \frac{1}{2\Gamma(v)\Gamma(\zeta)} \Gamma_{3,2}^{1,3} \left[\sqrt{\frac{\lambda}{\delta b^2 Q}} \middle| \begin{matrix} (0, \frac{1}{2}, \frac{Q}{P\lambda}), (1-\zeta, \frac{1}{2}), (1,1) \\ (v,1), (0,1) \end{matrix} \right]. \quad (23)$$

In addition, as $P \rightarrow \infty$, we have

$$P_e^{asy} \approx \frac{1}{2\Gamma(v)\Gamma(\zeta)} H_{3,2}^{1,3} \left[\sqrt{\frac{\lambda}{\delta b^2 Q}} \middle| \begin{matrix} (0, \frac{1}{2}), (1-\zeta, \frac{1}{2}), (1,1) \\ (v,1), (0,1) \end{matrix} \right]. \quad (24)$$

V. NUMERICAL RESULTS

In this section, we utilize the derived analytical expressions for the outage probability, the ergodic capacity, and the average BER to investigate numerically the performance of the RIS-assisted secondary network for various system parameters. The correctness of analytical expressions is validated by using extensive Monte-Carlo simulations⁴.

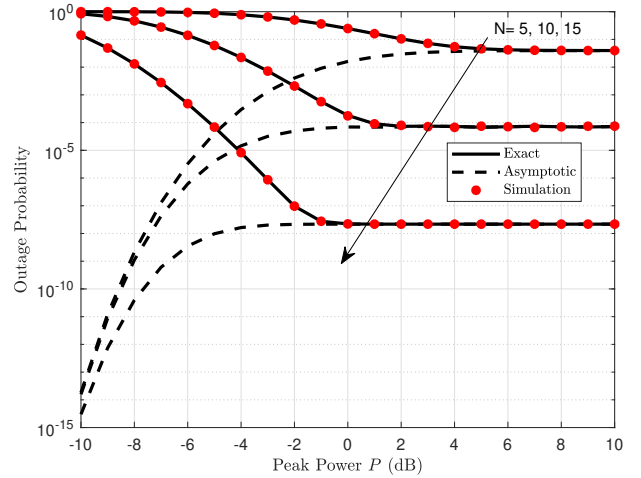


Fig. 2. Outage probability of the secondary network versus the SS peak power P for various values of RIS elements N at $\lambda = -5$ dB, $\gamma_{th} = 10$ dB, and $Q = 0$ dB.

It is worth mentioning that our analytical results hold true for arbitrarily chosen parameters. However, for the purpose of comparing the analytical results with the simulation results, we specifically consider the following settings, unless stated otherwise. In our simulations, we consider 10^7 independent samples (realizations) for performance evaluation. For the channel parameters of the secondary network, we take into consideration a Rician fading environment with the following parameters as in [17]: $v_1 = v_2 = 1$, $\sigma_1^2 = \sigma_2^2 = 0.5$ (i.e., the corresponding Rician factors are $K_1 = K_2 = 1$). In all figures, the analytical, asymptotic, and Monte-Carlo simulation results

⁴The incomplete H -function is not a built-in function in well-known software packages such as MATLAB and MATHEMATICA. Hence, we provide an efficient MATLAB code for evaluating the incomplete H -function at: <https://www.mathworks.com/matlabcentral/fileexchange/161176-incomplete-fox-h-function>.

are represented by solid lines, dashed lines, and markers only, respectively.

In Fig. 2, the outage probability of the secondary network is depicted against the SS peak power P for different values of RIS elements N . We first note that the exact outage probability in (7) precisely matches the Monte-Carlo simulations. Additionally, we observe that the asymptotic curves for the outage probability tend to converge to the exact curves as $P\lambda \gg Q$. As expected, the outage performance improves with increasing N . It is also evident that the outage performance exhibits saturation due to the peak power constraint at the SS.

Fig. 3 depicts the ergodic capacity versus the SS peak power P for different values of N . We note that the exact ergodic capacity in (10) matches perfectly with the Monte-Carlo simulations. Additionally, it can be observed that the asymptotic expression for ergodic capacity is highly accurate when $P\lambda \gg Q$. From this figure, it is evident that the ergodic capacity improves with increasing N or P , but it saturates as P grows large.

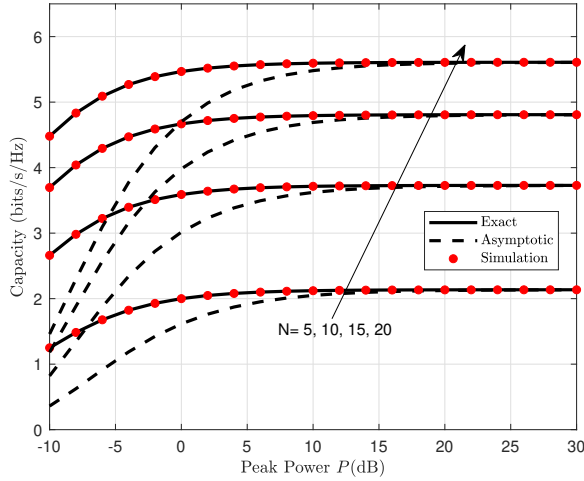


Fig. 3. Ergodic Capacity of the secondary network versus the SS peak power P for various values of RIS elements N at $\lambda = 0$ dB and $Q = -10$ dB.

Fig. 4 illustrates the ergodic capacity versus the interference power limit Q at the PR for different values of N . We observe that the exact ergodic capacity improves with increasing N , as expected. It is also evident that as the PR tolerates higher interference power (i.e., Q increases), the capacity improves. This is attributed to the fact that the SS transmit power increases with Q as shown in (3), leading to better performance. Additionally, we note that while the asymptotic ergodic capacity is highly accurate when $P\lambda \gg Q$, it diverges from the exact capacity as Q increases.

In Fig. 5, we plot the ergodic capacity versus N for various values of Q . We investigate the influence of increasing N on the ergodic capacity and validate the accuracy of our exact and asymptotic expressions through Monte-Carlo simulations. The observations about the asymptotic curve align with our discussion in previous figures.

Fig. 6, illustrates the average BER of binary phase shift keying (BPSK) modulation format versus P for different values of N . We first notice that the exact average BER in

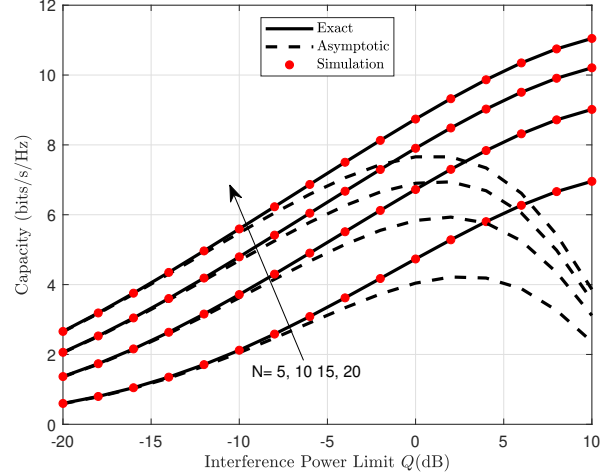


Fig. 4. Ergodic Capacity of the secondary network versus the interference power limit Q for various values of RIS elements N at $\lambda = 0$ dB and $P = 10$ dB.

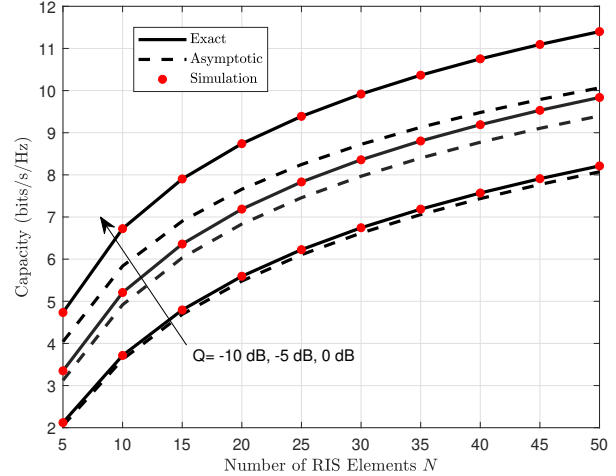


Fig. 5. Ergodic Capacity of the secondary network versus the number of RIS elements N for various values of Q at $\lambda = 0$ dB and $P = 10$ dB.

(15) matches perfectly with the Monte-Carlo simulations. It is evident from this figure that average BER improves by either increasing N or Q . Furthermore, we note that the asymptotic curves for the average BER tend to converge to the exact curves at large values of P .

VI. CONCLUSION

In this work, we proposed a novel RIS-assisted underlay spectrum sharing system, in which a secondary network assisted by an RIS shares the spectrum dedicated to a primary network. The performance of the RIS-assisted secondary network over Rician fading channels is investigated while considering a practical transmit power adaptation at the SS and an interference power constraint at the PR. Novel exact analytical expressions, in terms of the H -function and the incomplete H -function, are derived to quantify the outage performance, the error performance, and the ergodic capacity. Asymptotic

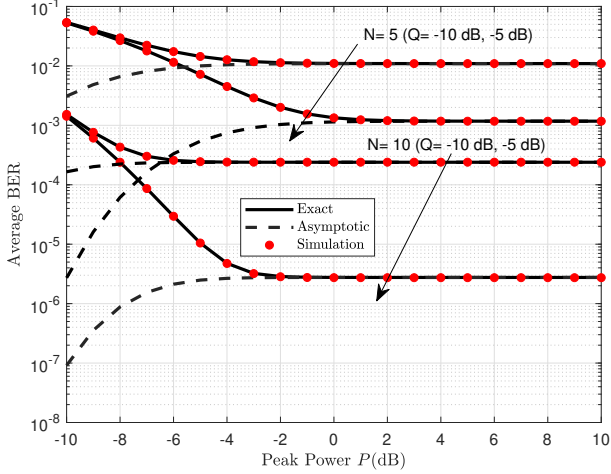


Fig. 6. Average BER of the secondary network versus the SS peak power P for various values of RIS elements N at $\lambda = -5$ dB.

expressions are also obtained for large values of the peak power of the SS. The derived results suggest that increasing the number of RIS elements N will substantially enhance the performance of the secondary network. In addition, our analytical approach is validated through extensive Monte-Carlo simulations.

APPENDIX A PROOF OF THEOREM 1

The CDF of ρ in (3) can be derived as

$$\begin{aligned} F_\rho(z) &= \Pr\{\rho \leq z\} \\ &= \Pr\left\{PR^2 \leq z, |h_0|^2 \leq \frac{Q}{P}\right\} \\ &\quad + \Pr\left\{\frac{QR^2}{|h_0|^2} \leq z, |h_0|^2 > \frac{Q}{P}\right\}. \end{aligned} \quad (25)$$

In view of $|h_0|^2$ and R^2 being independent RVs, $F_\rho(z)$ can be evaluated as

$$\begin{aligned} F_\rho(z) &= \Pr\left\{R^2 \leq \frac{z}{P}\right\} \Pr\left\{|h_0|^2 \leq \frac{Q}{P}\right\} \\ &\quad + \int_{\frac{Q}{P}}^{\infty} \Pr\left\{R^2 \leq \frac{zx}{Q}\right\} f_{|h_0|^2}(x) dx. \end{aligned} \quad (26)$$

Using the fact that $|h_0|^2$ is an exponential RV with mean λ , then $F_\rho(z)$ can be expressed in terms of the CDF of R^2 as

$$\begin{aligned} F_\rho(z) &= F_{R^2}\left(\frac{z}{P}\right) \left(1 - e^{-\frac{Q}{P\lambda}}\right) \\ &\quad + \int_{\frac{Q}{P}}^{\infty} F_{R^2}\left(\frac{zx}{Q}\right) \frac{1}{\lambda} e^{-\frac{x}{\lambda}} dx. \end{aligned} \quad (27)$$

Making use of (4) in (27) yields

$$\begin{aligned} F_\rho(z) &= \frac{\gamma\left(v, \sqrt{\frac{z}{b^2 P}}\right)}{\Gamma(v)} \left(1 - e^{-\frac{Q}{P\lambda}}\right) \\ &\quad + \underbrace{\int_{\frac{Q}{P}}^{\infty} \frac{\gamma\left(v, \sqrt{\frac{zx}{b^2 Q}}\right)}{\Gamma(v)} \frac{1}{\lambda} e^{-\frac{x}{\lambda}} dx}_{I_1}. \end{aligned} \quad (28)$$

We focus next on evaluating the integral expression I_1 in (28). The first step is to express the lower incomplete Gamma function in terms of the Meijer G -function as [48, Eq. (8.4.16.1)]

$$\begin{aligned} \gamma\left(v, \sqrt{\frac{zx}{b^2 Q}}\right) &= G_{1,2}^{1,1}\left(\sqrt{\frac{zx}{b^2 Q}} \middle| \begin{matrix} 1 \\ v, 0 \end{matrix}\right) \\ &= \frac{1}{2\pi j} \int_{\mathcal{L}} \frac{\Gamma(s)\Gamma(v-s)}{\Gamma(1+s)} \left(\frac{zx}{b^2 Q}\right)^{\frac{s}{2}} ds, \end{aligned} \quad (29)$$

where the second line in (29) represents the Mellin-Barnes integral of the Meijer G -function [45, Definition 1.5].

Plugging (29) into the integral expression of (28) will result in (31). The inner integral in (31) can be evaluated with the help of [43, Eq. (3.381.3)] as

$$I_2 = \int_{\frac{Q}{P}}^{\infty} x^{\frac{s}{2}} \frac{1}{\lambda} e^{-\frac{x}{\lambda}} dx = \lambda^{\frac{s}{2}} \Gamma\left(1 + \frac{s}{2}, \frac{Q}{P\lambda}\right). \quad (30)$$

Substituting (30) into (31) leads to (32). Considering (32) and using the definition of the incomplete H -function [42, Eq. (2.3)], $F_\rho(z)$ in (28) can be finally expressed in a compact form as in (5).

To this end, $f_\rho(z)$ is obtained as shown in (6) by differentiating $F_\rho(z)$ with respect to z with the help of [42, Eq. (2.12)]. This completes the proof of Theorem 1.

APPENDIX B PROOF OF THEOREM 2

The first step is to express $f_\rho(z)$ in (6) as

$$f_\rho(z) = f_\rho^{(1)}(z) + f_\rho^{(2)}(z). \quad (36)$$

Here, we consider $f_\rho^{(1)}(z) = \frac{z^{\frac{v}{2}-1} e^{-\sqrt{\frac{z}{b^2 P}}}}{2(b^2 P)^{\frac{v}{2}} \Gamma(v)} \left(1 - e^{-\frac{Q}{P\lambda}}\right)$ and

$$f_\rho^{(2)}(z) = \frac{z^{-1}}{\Gamma(v)} \Gamma_{3,3}^{1,3} \left[\sqrt{\frac{z\lambda}{b^2 Q}} \middle| \begin{matrix} (0, \frac{1}{2}, \frac{Q}{P\lambda}), (0, \frac{1}{2}), (1, 1) \\ (v, 1), (0, 1), (1, \frac{1}{2}) \end{matrix} \right].$$

We now evaluate $C^{(1)}$ as

$$C^{(1)} = \frac{1}{\ln(2)} \int_0^\infty \ln(1+z) f_\rho^{(1)}(z) dz. \quad (37)$$

Using the transformation of variables $u = \sqrt{\frac{z}{b^2 P}}$, the integral above can be expressed as

$$C^{(1)} = \frac{(1 - e^{-\frac{Q}{P\lambda}})}{\ln(2)\Gamma(v)} \int_0^\infty \ln(1 + b^2 P u^2) u^{v-1} e^{-u} du. \quad (38)$$

The term $\ln(1 + b^2 P u^2)$ can be written in terms of Meijer G -function as [48, Eq. (8.4.6.5)] as

$$\ln(1 + b^2 P u^2) = G_{2,2}^{1,2} \left(b^2 P u^2 \middle| \begin{matrix} 1, 1 \\ 1, 0 \end{matrix} \right). \quad (39)$$

To this end, substituting (39) in (38) and applying [45, Eq. (2.29)], $C^{(1)}$ can be finally expressed as in (11).

In what follows, we evaluate $C^{(2)}$ as

$$C^{(2)} = \frac{1}{\ln(2)} \int_0^\infty \ln(1+z) f_\rho^{(2)}(z) dz. \quad (40)$$

We first utilize [42, Eq. (2.3)] to express $f_\rho^{(2)}(z)$ in terms of the Mellin-Barnes integral as in (33).

$$I_1 = \frac{1}{2\pi j\Gamma(v)} \int_{\mathcal{L}} \frac{\Gamma(s)\Gamma(v-s) \left(\frac{z}{b^2Q}\right)^{\frac{s}{2}}}{\Gamma(1+s)} \underbrace{\left(\int_{\frac{Q}{P}}^{\infty} x^{\frac{s}{2}} \frac{1}{\lambda} e^{-\frac{x}{\lambda}} dx\right)}_{I_2} ds. \quad (31)$$

$$I_1 = \frac{1}{2\pi j\Gamma(v)} \int_{\mathcal{L}} \frac{\Gamma\left(1+\frac{s}{2}, \frac{Q}{P\lambda}\right) \Gamma(s)\Gamma(v-s) \left(\frac{z\lambda}{b^2Q}\right)^{\frac{s}{2}}}{\Gamma(1+s)} ds. \quad (32)$$

$$f_p^{(2)}(z) = \frac{z^{-1}}{2\pi j\Gamma(v)} \int_{\mathcal{L}} \frac{\Gamma\left(1+\frac{s}{2}, \frac{Q}{P\lambda}\right) \Gamma(s)\Gamma(v-s)\Gamma(1+\frac{s}{2}) \left(\frac{z\lambda}{b^2Q}\right)^{\frac{s}{2}}}{\Gamma(1+s)\Gamma(\frac{s}{2})} ds. \quad (33)$$

$$C^{(2)} = \frac{1}{2\pi j \ln(2)\Gamma(v)} \int_{\mathcal{L}} \frac{\Gamma\left(1+\frac{s}{2}, \frac{Q}{P\lambda}\right) \Gamma(s)\Gamma(v-s)\Gamma(1+\frac{s}{2}) \left(\frac{\lambda}{b^2Q}\right)^{\frac{s}{2}}}{\Gamma(1+s)\Gamma(\frac{s}{2})} \underbrace{\left(\int_0^{\infty} z^{\frac{s}{2}-1} \ln(1+z) dz\right)}_{I_3} ds. \quad (34)$$

$$C^{(2)} = \frac{1}{2\pi j \ln(2)\Gamma(v)} \int_{\mathcal{L}} \frac{\Gamma\left(1+\frac{s}{2}, \frac{Q}{P\lambda}\right) \Gamma(s)\Gamma(v-s)\Gamma(1-\frac{s}{2})\Gamma(\frac{s}{2}) \left(\frac{\lambda}{b^2Q}\right)^{\frac{s}{2}}}{\Gamma(1+s)} ds. \quad (35)$$

Plugging (33) into (40) will result in (34). The inner integral in (34) can be evaluated with the help of [43, Eq. (4.293.3)] as

$$I_3 = \int_0^{\infty} z^{\frac{s}{2}-1} \ln(1+z) dz = \frac{\pi}{\frac{s}{2} \sin\left(\frac{\pi s}{2}\right)}. \quad (41)$$

We now utilize [43, Eq. (8.334.3) and Eq. (8.331.1)] to express I_3 in terms of a product of gamma functions as

$$I_3 = \frac{\Gamma\left(1-\frac{s}{2}\right) \Gamma\left(\frac{s}{2}\right) \Gamma\left(\frac{s}{2}\right)}{\Gamma\left(1+\frac{s}{2}\right)}. \quad (42)$$

Making use of (42) in (34) leads to (35). Considering (35) and using the definition of the incomplete H -function [42, Eq. (2.3)], $C^{(2)}$ in (40) can be finally expressed in a compact form as in (12). This concludes Theorem 2.

APPENDIX C PROOF OF THEOREM 3

Consider the first and the second terms of $F_p(z)$ in (5) as $F_p^{(1)}(z)$ and $F_p^{(2)}(z)$, respectively. Then, $P_e^{(1)}$ can be expressed as

$$\begin{aligned} P_e^{(1)} &= \frac{\delta^\zeta}{2\Gamma(\zeta)} \int_0^{\infty} e^{-\delta z} z^{\zeta-1} F_p^{(1)}(z) dz \\ &= \frac{\left(1 - e^{-\frac{Q}{P\lambda}}\right) \delta^\zeta}{2\Gamma(v)\Gamma(\zeta)} \int_0^{\infty} e^{-\delta z} z^{\zeta-1} \gamma\left(v, \sqrt{\frac{z}{b^2P}}\right) dz. \end{aligned} \quad (43)$$

The lower incomplete Gamma function in the second line of (43) can be expressed in terms of the Meijer G -function as [48, Eq. (8.4.16.1)]

$$\gamma\left(v, \sqrt{\frac{z}{b^2P}}\right) = G_{1,2}^{1,1}\left(\sqrt{\frac{z}{b^2P}} \middle| \begin{matrix} 1 \\ v, 0 \end{matrix}\right). \quad (44)$$

Making use of (44) in (43) and utilizing the Laplace transform property of the Meijer G -function [45, Eq. (2.29)], $P_e^{(1)}$ is finally as given in (16).

Similarly, $P_e^{(2)}$ can be obtained from $F_p^{(2)}(z)$ as

$$\begin{aligned} P_e^{(2)} &= \frac{\delta^\zeta}{2\Gamma(\zeta)} \int_0^{\infty} e^{-\delta z} z^{\zeta-1} F_p^{(2)}(z) dz \\ &= \frac{\delta^\zeta}{2\Gamma(v)\Gamma(\zeta)} \int_0^{\infty} e^{-\delta z} z^{\zeta-1} \\ &\quad \times \Gamma_{2,2}^{1,2}\left[\sqrt{\frac{z\lambda}{b^2Q}} \middle| \begin{matrix} (0, \frac{1}{2}, \frac{Q}{P\lambda}), (1, 1) \\ (v, 1), (0, 1) \end{matrix}\right] dz. \end{aligned} \quad (45)$$

Considering (45) and utilizing the Laplace transform property of the incomplete H -function [42, Eq. (3.6)], $P_e^{(2)}$ is finally as given in (17). This completes the proof of Theorem 3.

REFERENCES

- [1] F. Boccardi, R. W. Heath, A. Lozano, T. L. Marzetta, and P. Popovski, "Five disruptive technology directions for 5g," *IEEE Communications Magazine*, vol. 52, no. 2, pp. 74–80, 2014.
- [2] S. Dang, O. Amin, B. Shihada, and M.-S. Alouini, "What should 6g be?" *Nature Electronics*, vol. 3, no. 1, pp. 20–29, 2020.

- [3] K. B. Letaief, W. Chen, Y. Shi, J. Zhang, and Y.-J. A. Zhang, "The roadmap to 6g: Ai empowered wireless networks," *IEEE Communications Magazine*, vol. 57, no. 8, pp. 84–90, 2019.
- [4] E. Basar, "Transmission through large intelligent surfaces: A new frontier in wireless communications," in *2019 European Conference on Networks and Communications (EuCNC)*, 2019, pp. 112–117.
- [5] M. D. Renzo, M. Debbah, D.-T. Phan-Huy, A. Zappone, M.-S. Alouini, C. Yuen, V. Sciancalepore, G. C. Alexandropoulos, J. Hoydis, H. Gacanin *et al.*, "Smart radio environments empowered by reconfigurable ai meta-surfaces: An idea whose time has come," *EURASIP Journal on Wireless Communications and Networking*, vol. 2019, no. 1, pp. 1–20, 2019.
- [6] C. Liaskos, S. Nie, A. Tsioliaridou, A. Pitsillides, S. Ioannidis, and I. Akyildiz, "A new wireless communication paradigm through software-controlled metasurfaces," *IEEE Communications Magazine*, vol. 56, no. 9, pp. 162–169, 2018.
- [7] G. Lavigne, K. Achouri, V. S. Asadchy, S. A. Tretyakov, and C. Caloz, "Susceptibility derivation and experimental demonstration of refracting metasurfaces without spurious diffraction," *IEEE Transactions on Antennas and Propagation*, vol. 66, no. 3, pp. 1321–1330, 2018.
- [8] C. Liaskos, S. Nie, A. Tsioliaridou, A. Pitsillides, S. Ioannidis, and I. Akyildiz, "Realizing wireless communication through software-defined hypersurface environments," in *2018 IEEE 19th International Symposium on "A World of Wireless, Mobile and Multimedia Networks" (WoWMoM)*, 2018, pp. 14–15.
- [9] F. Liu, A. Pitolakis, M. S. Mirmoosa, O. Tsilipakos, X. Wang, A. C. Tasolamprou, S. Abadal, A. Cabellos-Aparicio, E. Alarcón, C. Liaskos, N. V. Kantartzis, M. Kafesaki, E. N. Economou, C. M. Soukoulis, and S. Tretyakov, "Programmable metasurfaces: State of the art and prospects," in *2018 IEEE International Symposium on Circuits and Systems (ISCAS)*, 2018, pp. 1–5.
- [10] E. Basar, M. Di Renzo, J. De Rosny, M. Debbah, M.-S. Alouini, and R. Zhang, "Wireless communications through reconfigurable intelligent surfaces," *IEEE Access*, vol. 7, pp. 116 753–116 773, 2019.
- [11] L. Yang, F. Meng, Q. Wu, D. B. da Costa, and M.-S. Alouini, "Accurate closed-form approximations to channel distributions of ris-aided wireless systems," *IEEE Wireless Communications Letters*, vol. 9, no. 11, pp. 1985–1989, 2020.
- [12] I. Trigui, W. Ajib, W.-P. Zhu, and M. D. Renzo, "Performance evaluation and diversity analysis of ris-assisted communications over generalized fading channels in the presence of phase noise," *IEEE Open Journal of the Communications Society*, vol. 3, pp. 593–607, 2022.
- [13] A.-A. A. Boulogeorgos and A. Alexiou, "Performance analysis of reconfigurable intelligent surface-assisted wireless systems and comparison with relaying," *IEEE Access*, vol. 8, pp. 94 463–94 483, 2020.
- [14] T. Wang, G. Chen, M.-A. Badiu, and J. P. Coon, "Performance analysis of RIS-assisted large-scale wireless networks using stochastic geometry," *IEEE Transactions on Wireless Communications*, pp. 1–1, 2023.
- [15] Q. Tao, J. Wang, and C. Zhong, "Performance analysis of intelligent reflecting surface aided communication systems," *IEEE Communications Letters*, vol. 24, no. 11, pp. 2464–2468, 2020.
- [16] I. Yildirim, A. Uyrus, and E. Basar, "Modeling and analysis of reconfigurable intelligent surfaces for indoor and outdoor applications in future wireless networks," *IEEE Transactions on Communications*, vol. 69, no. 2, pp. 1290–1301, 2021.
- [17] A. M. Salhab and M. H. Samuh, "Accurate performance analysis of reconfigurable intelligent surfaces over rician fading channels," *IEEE Wireless Communications Letters*, vol. 10, no. 5, pp. 1051–1055, 2021.
- [18] P. Xu, W. Niu, G. Chen, Y. Li, and Y. Li, "Performance analysis of ris-assisted systems with statistical channel state information," *IEEE Transactions on Vehicular Technology*, vol. 71, no. 1, pp. 1089–1094, 2022.
- [19] T. Bao, H. Wang, H.-C. Yang, W.-J. Wang, and M. O. Hasna, "Performance analysis of ris-aided communication systems over the sum of cascaded rician fading with imperfect csi," in *2022 IEEE Wireless Communications and Networking Conference (WCNC)*, 2022, pp. 399–404.
- [20] S. Hu, Z. Wei, Y. Cai, C. Liu, D. W. K. Ng, and J. Yuan, "Robust and secure sum-rate maximization for multiuser MISO downlink systems with self-sustainable IRS," *IEEE Transactions on Communications*, vol. 69, no. 10, pp. 7032–7049, 2021.
- [21] Y.-W. Chen, R. Zhang, C.-W. Hsu, and G.-K. Chang, "Key enabling technologies for the post-5g era: Fully adaptive, all-spectra coordinated radio access network with function decoupling," *IEEE Communications Magazine*, vol. 58, no. 9, pp. 60–66, 2020.
- [22] H. Van Toan and V. N. Q. Bao, "Performance analysis of cognitive two-way networks with interference from primary user over nakagami-m fading channels," *Journal of Science and Technology: Issue on Information and Communications Technology*, vol. 3, no. 1, pp. 29–37, 2017.
- [23] A. Rezaee and V. W. S. Chan, "Cognitive network management and control with significantly reduced state sensing," *IEEE Transactions on Cognitive Communications and Networking*, vol. 5, no. 3, pp. 783–794, 2019.
- [24] A. Goldsmith, S. A. Jafar, I. Maric, and S. Srinivasa, "Breaking spectrum gridlock with cognitive radios: An information theoretic perspective," *Proceedings of the IEEE*, vol. 97, no. 5, pp. 894–914, 2009.
- [25] L. Zhang, Y. Wang, W. Tao, Z. Jia, T. Song, and C. Pan, "Intelligent reflecting surface aided mimo cognitive radio systems," *IEEE Transactions on Vehicular Technology*, vol. 69, no. 10, pp. 11 445–11 457, 2020.
- [26] J. Yuan, Y.-C. Liang, J. Joung, G. Feng, and E. G. Larsson, "Intelligent reflecting surface-assisted cognitive radio system," *IEEE Transactions on Communications*, vol. 69, no. 1, pp. 675–687, 2021.
- [27] N. D. Nguyen, A.-T. Le, and M. Munochiveyi, "Secrecy outage probability of reconfigurable intelligent surface-aided cooperative underlay cognitive radio network communications," in *2021 22nd Asia-Pacific Network Operations and Management Symposium (APNOMS)*, 2021, pp. 73–77.
- [28] L. Dong, H.-M. Wang, and H. Xiao, "Secure cognitive radio communication via intelligent reflecting surface," *IEEE Transactions on Communications*, vol. 69, no. 7, pp. 4678–4690, 2021.
- [29] D. Xu, X. Yu, Y. Sun, D. W. K. Ng, and R. Schober, "Resource allocation for iris-assisted full-duplex cognitive radio systems," *IEEE Transactions on Communications*, vol. 68, no. 12, pp. 7376–7394, 2020.
- [30] A. U. Makarfi, R. Kharel, K. M. Rabie, O. Kaiwartya, X. Li, and D.-T. Do, "Reconfigurable intelligent surfaces based cognitive radio networks," in *2021 IEEE Wireless Communications and Networking Conference Workshops (WCNCW)*, 2021, pp. 1–6.
- [31] L. Zhang, C. Pan, Y. Wang, H. Ren, and K. Wang, "Robust beamforming design for intelligent reflecting surface aided cognitive radio systems with imperfect cascaded csi," *IEEE Transactions on Cognitive Communications and Networking*, vol. 8, no. 1, pp. 186–201, 2022.
- [32] K. Guo, R. Liu, M. Alazab, R. H. Jhaveri, X. Li, and M. Zhu, "STAR-RIS-empowered cognitive non-terrestrial vehicle network with noma," *IEEE Transactions on Intelligent Vehicles*, pp. 1–15, 2023.
- [33] P. Yang, L. Yang, W. Kuang, and S. Wang, "Outage performance of cognitive radio networks with a coverage-limited RIS for interference elimination," *IEEE Wireless Communications Letters*, vol. 11, no. 8, pp. 1694–1698, 2022.
- [34] S. Ghose, D. Mishra, S. P. Maity, and G. C. Alexandropoulos, "RIS reflection and placement optimisation for underlay d2d communications in cognitive cellular networks," in *ICASSP 2023 - 2023 IEEE International Conference on Acoustics, Speech and Signal Processing (ICASSP)*, 2023, pp. 1–5.
- [35] Y. H. Al-Badarnah, A. Elzanaty, and M.-S. Alouini, "On the performance of spectrum-sharing backscatter communication systems," *IEEE Internet of Things Journal*, vol. 9, no. 3, pp. 1951–1961, 2022.
- [36] Z. Ding and H. Vincent Poor, "A simple design of IRS-NOMA transmission," *IEEE Communications Letters*, vol. 24, no. 5, pp. 1119–1123, 2020.
- [37] S. Atapattu, R. Fan, P. Dharmawansa, G. Wang, J. Evans, and T. A. Tsiftsis, "Reconfigurable intelligent surface assisted two-way communications: Performance analysis and optimization," *IEEE Transactions on Communications*, vol. 68, no. 10, pp. 6552–6567, 2020.
- [38] T. W. Ban, W. Choi, B. C. Jung, and D. K. Sung, "Multi-user diversity in a spectrum sharing system," *IEEE Transactions on Wireless Communications*, vol. 8, no. 1, pp. 102–106, 2009.
- [39] L. Wei, C. Huang, G. C. Alexandropoulos, C. Yuen, Z. Zhang, and M. Debbah, "Channel estimation for RIS-empowered multi-user MISO wireless communications," *IEEE Transactions on Communications*, vol. 69, no. 6, pp. 4144–4157, 2021.
- [40] Y. Xu, H. Chu, and P. Xu, "Joint channel estimation and passive beamforming for reconfigurable intelligent surface aided multi-user massive MIMO system," in *2021 IEEE International Black Sea Conference on Communications and Networking (BlackSeaCom)*, 2021, pp. 1–3.
- [41] A. Jeffrey and D. Zwillinger, *Table of integrals, series, and products*. Academic Press, 2007.
- [42] H. Srivastava, R. Saxena, and R. Parmar, "Some families of the incomplete H-functions and the incomplete H-functions and associated integral transforms and operators of fractional calculus with applications," *Russian Journal of Mathematical Physics*, vol. 25, no. 1, pp. 116–138, 2018.
- [43] I. S. Gradshteyn and I. M. Ryzhik, *Table of integrals, series, and products*. Academic press, 2014.

- [44] J. Proakis and M. Salehi, *Digital Communications*. McGraw-Hill, 2008.
- [45] A. M. Mathai, R. K. Saxena, and H. J. Haubold, *The H-function: theory and applications*. Springer Science & Business Media, 2009.
- [46] I. S. Ansari, S. Al-Ahmadi, F. Yilmaz, M.-S. Alouini, and H. Yanikomeroglu, "A new formula for the BER of binary modulations with dual-branch selection over generalized-k composite fading channels," *IEEE Transactions on Communications*, vol. 59, no. 10, pp. 2654–2658, 2011.
- [47] S. Meena, S. Bhattar, K. Jangid, and S. D. Purohit, "Some expansion formulas for incomplete h-and h-functions involving bessel functions," *Advances in Difference Equations*, vol. 2020, no. 1, p. 562, 2020.
- [48] A. Prudnikov, Y. Brychkov, and O. Marichev, "Integrals series: More special functions, volume III of integrals and series," *New York: Gordon and Breach Science Publishers*, 1990.



Yazan H. Al-Badarnah was born in Irbid, Jordan, in 1987. He obtained his Ph.D. in Electrical Engineering from Texas A&M University, College Station, TX, USA, in 2018. Following his graduation, he joined the Department of Electrical Engineering at The University of Jordan, Amman, Jordan, as an Assistant Professor. In September 2023, in recognition of his academic contributions, he was promoted to the rank of Associate Professor within the same department. Since September 2023, he has been serving as a Deputy Dean for Quality Affairs,

Accreditation, and Ranking at the School of Engineering, The University of Jordan. His scholarly pursuits predominantly focus on the application of information and communication theories to contemporary wireless communication systems, with particular emphasis on modeling, design, and performance analysis.



Mustafa Alshawaqfeh received his Ph.D. degree in Electrical Engineering from Texas A&M University, College Station, Texas, USA, in 2017, M.S., degree in wireless communication from the Jordan University of Science and Technology, Irbid, Jordan, in 2010, and B.S. degree in communication engineering from Yarmouk University, Irbid, Jordan, in 2007. He joined the German Jordanian University in 2017 as an Assistant Professor. In September 2021, He was promoted to an Associate Professor in the EE department. His research interests span

the areas of wireless communications, signal processing, machine learning, and bioinformatics. In the area of wireless communication, he worked on (i) applying signal processing, mainly sparse recovery and tree search algorithms, to develop efficient low complexity receivers especially for spatial modulation schemes and non-orthogonal multiple access (NOMA) systems, and (ii) analyzing the performance of wireless MIMO systems over fading channels. In the area of bioinformatics, he is working on applying signal processing and machine learning techniques to analyze biological datasets with the focus on developing algorithms for metagenomic biomarker detection.



Osamah S. Badarneh received his PhD in Electrical Engineering from the University of Quebec-École de Technologie Supérieure (ETS), Canada, in 2009. He joined the German Jordanian University (GJU) in 2018 and he is currently a Full Professor with the Department of Electrical Engineering. He served as an Adjunct Professor with the Department of Electrical Engineering, University of Quebec-ETS, 2013-2018. From 2012 to 2018, he was an Associate Professor with the Department of Electrical Engineering, University of Tabuk. Also, he worked as an Assistant Professor with the Department of Telecommunication Engineering, Yarmouk University, from 2010 to 2012. His research interests focus on wireless communications and networking. He is the author of more than 100 publications in scientific journals and international conferences.



Yazid M. Khattabi received the bachelor's degree in electrical engineering with a specialization in electronics and communications and the master's degree in electrical engineering with a specialization in wireless communications both from Jordan University of Science and Technology (JUST), Irbid, Jordan, in 2008 and 2010, respectively, and the Ph.D. degree in electrical engineering with a specialization in wireless communications from the Center for Wireless Communications (CWC), University of Mississippi, Oxford, MS, USA, in 2016. From

March 2011 to December 2012, he served as a telecommunications and electronics design engineer at King Abdullah II Design and Development Bureau (KADDB), Amman, Jordan, with responsibilities included and not limited to telecommunication systems design for unmanned vehicles; electronics and RF printed circuits software design, implementation, and maintenance; RF planning & optimization; signal propagation modeling; etc. From 2013 to 2016, he served as a research assistant with the CWC, University of Mississippi, where he received several research awards. Since August, 2016, he has been with the University of Jordan, Amman, Jordan, where he is currently an Associate Professor of electrical engineering. His current research interests include several areas in wireless communications with emphasis on performance evaluation and optimization of backscatter communications, reconfigurable intelligent surfaces (RIS) communications, relaying and cooperative communications, cognitive radio based communications, MIMO and spatial modulation (SM) communications, high-speed-railway communications, wireless powered communications, internet of things (IoT) communications, lightweight encryption algorithms, vehicular and unmanned-aerial-vehicle (UAV) communications, mm-wave and Tera-Hz communications. He is also serving as a reviewer for several refereed international journals and conferences.